Study on microstructure and friction and wear properties of wear-resistant coatings prepared by thermal spraying

Z. L. Wang[a], Q. Li[b], Q. X. Li[b], C. Ju[a], Q. H. Song[a], J. J. Li[a], Z. P. Sun[a], Y. F. Zhang[a,*]

[a]*School of Mechanical & Automotive Engineering, Qilu University of Technology (Shandong Academy of Sciences), Jinan, Shandong, 250353, PR China*
[b]*School of Material Science & Engineering, Qilu University of Technology (Shandong Academy of Sciences), Jinan, Shandong, 250353, PR China*

In this paper, Cr_2O_3-$2TiO_2$ and Al_2O_3 coatings are prepared by atmospheric plasma spraying (APS), and WC-10Co4Cr was prepared by high velocity oxygen fuel (HVOF). The powders and coatings are characterized with scanning electron microscopy (SEM) and energy dispersive spectrometry. X-ray diffraction (XRD) is used to qualitatively analyze the phase. The generation of new material is analyzed. The Vickers hardness of each coating is tested by microhardness tester. The tribological properties of the coatings are tested with the multifunctional material surface tester and the friction coefficient curves are drawn with the collected data. It is found that the friction and wear properties of the Cr_2O_3-$2TiO_2$ coating are good due to the high degree of flattening during spraying. Cr_2O_3-$2TiO_2$ coating has the highest average hardness. The phase structure is stable before and after spraying. Compared with the powder, the X-ray diffraction peaks of Al_2O_3 coating are seriously widened, some diffraction peaks are offset, and the intensity of the derived peaks is significantly reduced. Al_2O_3 coating has the largest hardness and lowest average hardness. However, compared with the other two coatings, Al_2O_3 coating has the worst wear resistance. It is also found that decarburization occurred during HVOF of WC-10Co4Cr. However, CoCr phase will wrap the WC, which can greatly reduce decarburization of WC during spraying. The bonding strength, wear resistance and toughness of the coating will be significantly enhanced. Compared with Al_2O_3 coating and Cr_2O_3-$2TiO_2$ coating, the wear resistance of WC-10Co4Cr coating is slightly better.

---

* Corresponding author: zhangyanfei@qlu.edu.cn

1. Introduction

Friction and wear are common phenomena in nature. Friction occurs when surfaces of objects come into contact and move relative to each other. Friction is accompanied by wear. Wear will not only lead to mechanical equipment parts damage and failure, but also consume a lot of resource[1]. With the continuous development of science and technology and the rapid rise of modern industry, the requirements of mechanical parts for their surface wear resistance are increasingly demanding[2]. In order to further improve the wear resistance of mechanical parts surface, it is of great significance to research and develop the preparation technology of wear-resistant coating[3]. The preparation and application of wear-resistant coatings can enable the mechanical equipment to operate stably in a variety of parameters and extreme environments for a long time and effectively extend its service life[4]. Coating technology can greatly change the wear resistance of the material surface and obtain the required wear-resistant coating. The wear-resistant coatings obtained by strengthening and modifying the surface of materials are more and more widely used in the fields of cutting-edge technology such as aerospace, atomic energy equipment, machinery and electronics[5].

Thermal spraying technology has the characteristics of flexible process, wide application range, small heating area and high production efficiency[6-7]. Coatings prepared by thermal spraying technology have high binding strength and excellent wear resistance, so they are more and more widely used in the preparation and application of wear-resistant coatings[8]. Plasma-spraying process is a fast coating deposition process having rapid heating and cooling rates, which are beneficial to deposit coatings[9].

Cr_2O_3 coating prepared by plasma spraying has high hardness, moderate thermal conductivity and good tribological properties[10]. After adding appropriate proportion of TiO_2 into Cr_2O_3 powder, plasma sprayed Cr_2O_3-TiO_2 composite coating is not only as hard as single Cr_2O_3 coating, but also has better toughness[11].

Al_2O_3 coating has the characteristics of high hardness, wear resistance, oxidation resistance and good chemical stability. It still shows excellent wear resistance in harsh environment. It is widely used as wear-resistant coating. It is also one of the earliest and most widely used ceramic coatings.

WC is the most commonly used cemented carbide, and Co is the most ideal binder. As coating materials, WC and Co constitute a synergistic and mutually reinforcing system[12-13]. Therefore, WC-Co system materials have excellent wear resistance[14-16]. In recent years, HVOF technology has been widely used to prepare WC-Co based dense coatings with high hardness and wear resistance. In order to improve the corrosion resistance of WC-Co coating, Cr element is often introduced into the coating system to form WC-Co-Cr coating system [17-18].

2. Methods and procedure

2.1. Preparation of coating

The feedstock powders of Cr_2O_3-$2TiO_2$ powder (Metco 106F) was obtained from Oerlikon Metco (Winterthur, Switzerland). The feedstock powders of Al_2O_3 powder and Ni-Al

powder were obtained from Jinzhou Jinjiang spraying material Co., Ltd (Liaoning, China). The feedstock powders of WC-10Co4Cr powder was obtained from Chengdu large solar thermal spraying material Co., Ltd (Sichuan, China). The composite coatings were fabricated by atmospheric plasma spraying (APS) and high velocity oxygen fuel (HVOF). Before spraying, the substrates (45 steel) were sand blasted with corundum grits and then cleaned by ultrasonic cleaner with acetone. Cr_2O_3-$2TiO_2$ and WC-10Co4Cr powders were sprayed directly onto the processed substrate. As for Al_2O_3 bond coat was plasma sprayed with Ni-Al powders. Afterwards, Al_2O_3 powders were deposited onto the surfaces of the bond coat using the APS process. The process parameters of Cr_2O_3-$2TiO_2$ coating is shown in Table 1. The process parameters of Al_2O_3 coating and bond coat are shown in Table 2. The process parameters of WC-10Co4Cr coating is shown in Table 3.

Table 1. Process parameters of plasma spraying Cr_2O_3-$2TiO_2$.

Powder	Cr_2O_3-$2TiO_2$
Current (A)	500
Voltage (V)	68
Primary gas pressure (Ar,PSI)	75
Primary gas flow (Ar,SCFH)	80
Power feed rate (% r.p.m)	25
Spray distance (mm)	75

Table 2. Process parameters of plasma spraying Al_2O_3 and bond coat.

Powder	Ni-Al	Al_2O_3
Current (A)	590	610
Voltage (V)	60	70
Primary gas pressure (MPa)	0.85	0.85
Primary gas flow (L·min⁻¹)	34	40
Power feed rate (r·min⁻¹)	4.3	7.3
Spray distance (mm)	150	130

Table 3. HVOF process parameters of WC-10Co4Cr.

Powder	WC-10Co4Cr
Kerosene pressure (MPa)	0.5
Oxygen pressure (MPa)	0.5
Hydrogen pressure (MPa)	0.5
Carrier gas flow (L·min⁻¹)	6
Powder feed rate/ (g·min⁻¹)	90
Spray distance (mm)	300

The X-ray diffraction (XRD) patterns of the samples were obtained on D8-ADVANCE (AXS, Germany). GeminiSEM500/VP (CARL ZEISS, Germany) ultrahigh resolution emission scanning electron microscope (SEM) was used to observe the surface microstructure of the powder and coating before and after spraying. The powders and coatings were impregnated with epoxy. After hardening of the resin, the sample was ground with SiC abrasive paper and polished on soft disks with diamond suspension. A cross section of the sample was investigated by SEM and Digital Microscope VHX-5000 (KEYENCE, Japan). The hardness of each coating was tested by HXD-1000TM microhardness tester. The microhardness of the coating was tested by a HXD-1000TM microhardness tester manufactured by Shanghai Taiming Optical Instrument Co., Ltd (China). The microhardness of the coatings was measured using a HXD-1000TM digital hardness tester under a load of 0.98 N with a dwell time of 15 s. At least ten measurements were performed on each sample. The friction and wear characteristics of the coating were tested on the MFT-4000 multifunctional tester for material surface manufactured by Lanzhou Huahui Instrument Technology Co., Ltd (Lanzhou, China). The coating surface was ground and polished prior to the test, and the coating was weighed and recorded using an XSR analytical balance manufactured by METTLER TOLEDO (Zurich, Switzerland). The readability of the XSR analytical balance ranges from 0.01 to 0.1mg with a maximum range of 320g. The friction test was carried out by reciprocating friction at room temperature. GCr15 alloy ball and Si_3N_4 ball with a diameter of 4 mm were selected as the grinding pairs. The coating sample was $1.5 \times 1 \times 0.2$mm, the reciprocating friction distance was 5mm, and the normal load was 10N. When the wear pair adopted GCr15 alloy ball, the wear time was 30 min, the friction frequency is 100 mm/min; when the Si_3N_4 ball was used for the wear pair, the wear time was 120 min, the friction frequency is 150 mm/min. After the test, the coating surface shall be cleaned and reweighed.

3. Result and discussion

3.1. Cr_2O_3-2TiO_2 (Metco 106F)

3.1.1. Morphology and composition of Cr_2O_3-2TiO_2 powder surface and section

Figure 1 shows the surface morphology and cross section of Cr_2O_3-2TiO_2 (Metco 106F) powder prepared by fusing and crushing. It can be seen from Figure 1a that the size of Cr_2O_3-2TiO_2 powder particles is different, mainly in the shape of block. It can also be seen that the powder is sintered and some of the sintered broken particles are irregular. Figure 1c shows the EDS element mapping of Cr_2O_3-2TiO_2 powder. It shows that the main composition of the powder is Cr_2O_3 with a little TiO_2. Figure 1d shows the SEM images of Cr_2O_3-2TiO_2 powders cross section. It can be seen that the powder is irregular with different particle sizes and broken shape.

Fusing and crushing method is a method of making ingot by melting raw materials, and then obtaining powder by mechanical crushing. Because of the high melting point of most oxides and carbides, it is impossible to use atomization method to prepare powders. However, these materials are brittle and easy to be broken. Therefore, fusing and crushing method is often used to prepare powders of these materials.
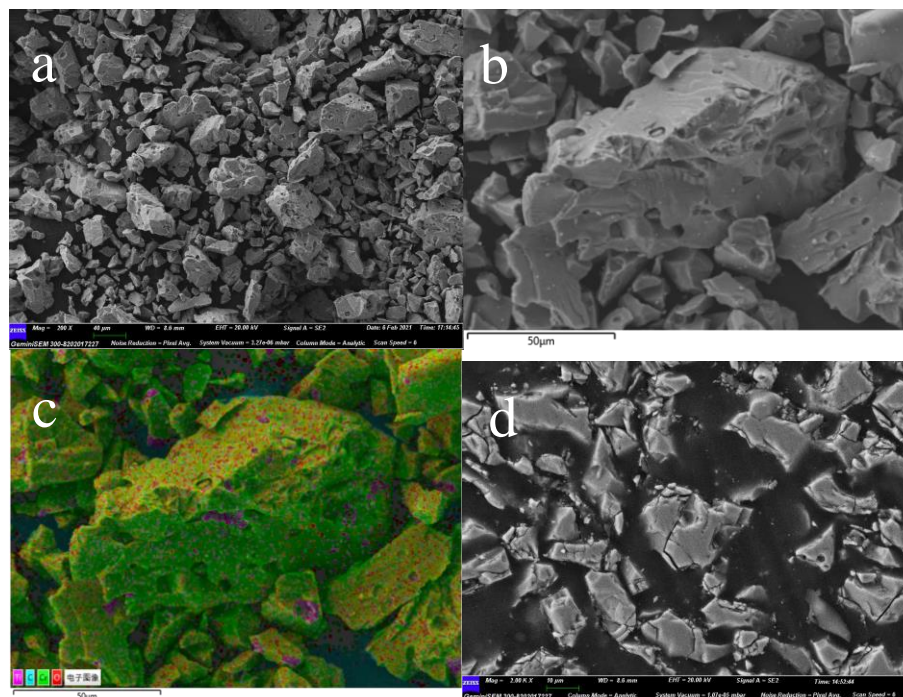
Fig. 1. SEM micrographs of Cr$_2$O$_3$-2TiO$_2$ powder.

3.1.2. Surface morphology and composition of Cr$_2$O$_3$-2TiO$_2$ coatings

Figure 2 shows the surface morphology of Cr$_2$O$_3$-2TiO$_2$ coating. It can be seen from Figure 2a that it is a typical plasma-sprayed coating. The surface of the coating consists of melted and unmelted particles. The particles spread well and the flattening degree is high. It can be seen from Figure 2b that the surface of the coating is undulating and loose due to the presence of unmelted particles. There are many pores on the coating surface (Figure 2c). The wavy pores are the interlaminar pores caused by insufficient overlap between lamellae, while the near-spherical pores are the internal pores caused by gas being sucked into the coating by sedimentary particles. Due to the quenching stress and thermal mismatch stress caused by the solidification shrinkage of droplets, there are fine cracks in the coating[10]. Figure 2d shows the EDS element mapping of Cr$_2$O$_3$-2TiO$_2$ coating. It can be seen that the surface composition of the coating is uniform, mainly Cr$_2$O$_3$.
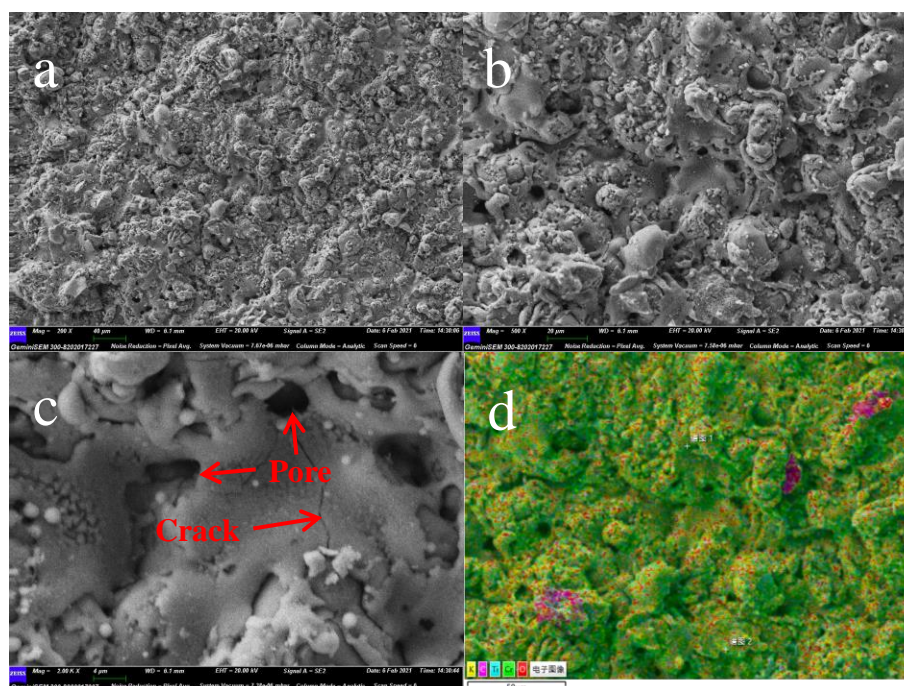
Fig. 2. SEM images of of Cr$_2$O$_3$-2TiO$_2$ coating surface morphology.

3.1.3. Cross section of Cr$_2$O$_3$-2TiO$_2$ coatings

Figure 3 shows the image of Cr$_2$O$_3$-2TiO$_2$ coating cross-section. The cross section of the coating is a typical layered stacking structure (Figure 3b-c). This is due to the spreading effect when the melted ceramic powder impacts on the substrate. There are a few pores between the layered structures. This may be due to the incomplete melting of particles, resulting in insufficient deformation, incomplete overlap, and the appearance of pores in the non overlapping area. The gas solubility in the molten particles decreases and gas gradually precipitates from the liquid phase with the decrease of temperature in the process of particles changing from liquid to solid. When the precipitated gas can not escape from the surface in time, it will stay in the coating and form pores[19]. Figure 3d shows the EDS element mapping of Cr$_2$O$_3$-2TiO$_2$ coating cross section. It can be seen that the main composition of the coating is Cr$_2$O$_3$, indicating that the composition is stable during spraying.
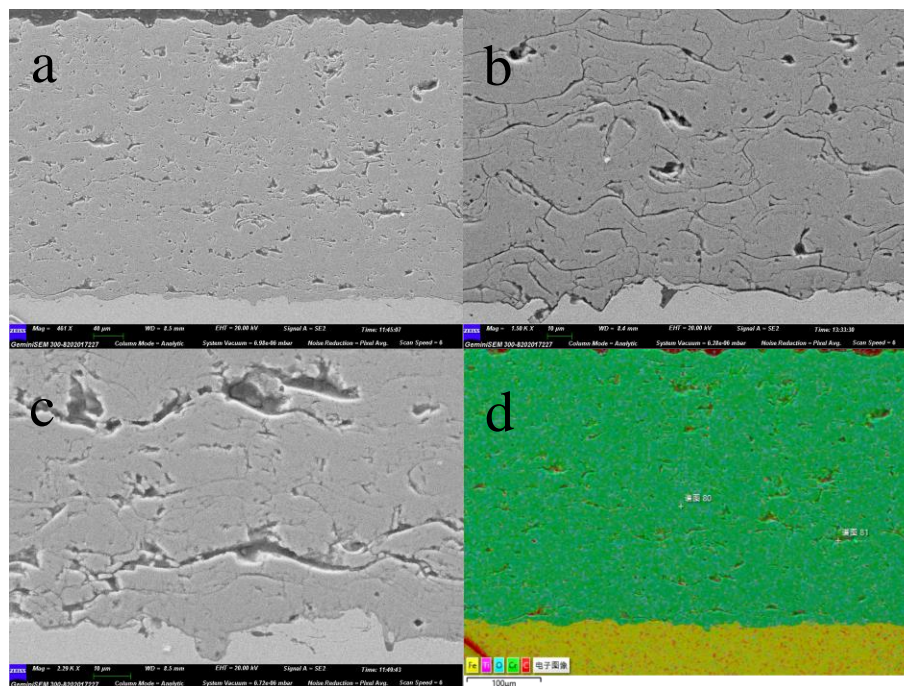
Fig. 3. Cross-section of Cr$_2$O$_3$-2TiO$_2$ coating.

3.1.4. XRD analysis of Cr$_2$O$_3$-2TiO$_2$

Figure 4 shows the XRD pattern of Cr$_2$O$_3$-2TiO$_2$ powder and coating prepared by APS, as well as the standard card of Cr$_2$O$_3$ (PDF#38-1479) for references. The analysis show that the main phase in the powder and coating is Cr$_2$O$_3$. Compared with powder, there is a new peak at 44.39° in coating, which is still Cr$_2$O$_3$ (PDF#38-1479). The phase composition of the powder and coating does not change much, which is mainly related to the properties of the material itself. In addition, the diffraction peaks do not shift, which indicates that the material does not undergo severe lattice expansion or contraction. There is a small amount of TiO$_2$ phase in the coating, and no diffraction peaks of other phases are found. This is because the crystal structure of green chromite Cr$_2$O$_3$ is the same as that of α-Al$_2$O$_3$. When the coating is prepared by plasma spraying, its structure remains stable without phase transformation[19]. The diffraction peaks characteristic of TiO$_2$ and Ti oxides were not found in the coating because the TiO$_2$ content was small or covered by the diffraction peaks of Cr$_2$O$_3$[20].
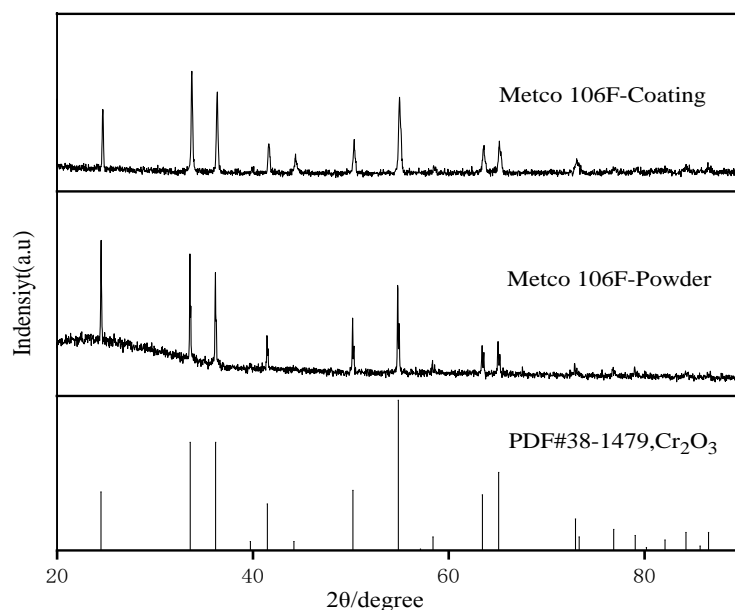
Fig. 4. XRD spectra of Cr_2O_3-$2TiO_2$ coating and powder.

3.2. Al_2O_3

3.2.1. Morphology and composition of Al_2O_3 powder surface and section

Figure 5 shows the surface and cross section morphology of Al_2O_3 powder prepared by high temperature melting. It can be seen from Figure 5a that Al_2O_3 particles are sintered together. The particles vary in size and are mainly massive. In the high magnification figure (Figure 5b), it can be observed that there will be fine and white attachments on the particles, and some surfaces have striped fluctuations, and there are unmelted or semi-molten particles on the surface. The EDS element mapping of the powder shows that there are almost no other compositions in Al_2O_3 powder.
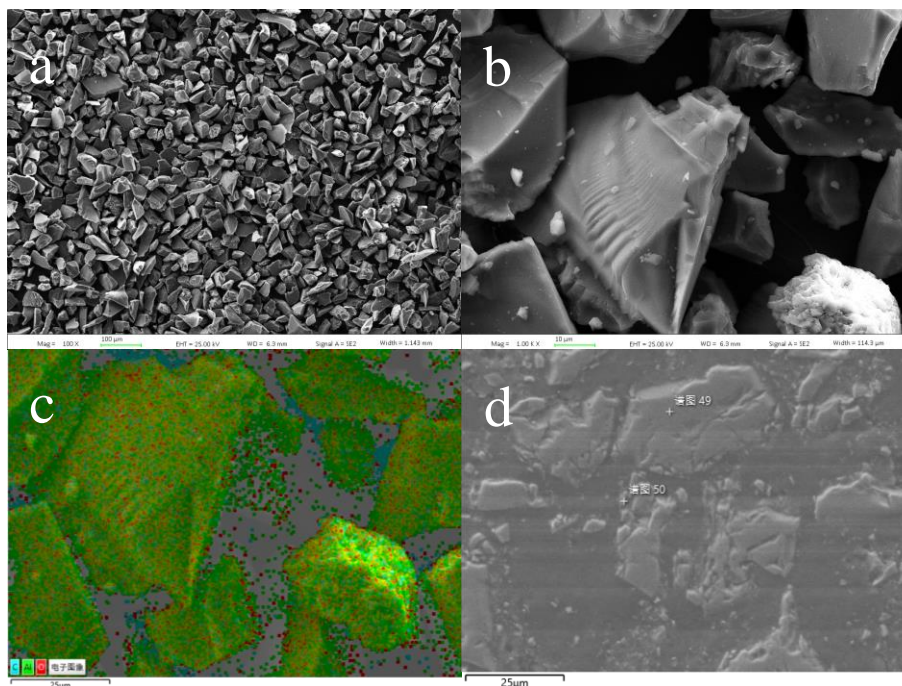

Fig. 5. SEM micrographs of Al_2O_3 powder.

3.2.2. Surface morphology and composition of Al₂O₃ coatings

Figure 6 shows the surface morphology of Al₂O₃ coating. It can be seen that Al₂O₃ coating also has the stacking structure of plasma-sprayed coating. There is a lamellar structure in the coating, which is due to the high temperature and speed of plasma spraying flame flow. When the particles impact the substrate surface at high speed in a molten state, they deform and form a lamellar structure during rapid cooling and solidification[21]. It can be seen from the low magnification figure (Figure 6a) that the surface of Al₂O₃ coating is relatively flat and the density is high. This is because the powder with high flame temperature and small particle size can be melted and deposited on the substrate surface[22]. Under the high magnification figure (Figure 6c), it can be seen that there are mostly semi-molten and unmelted particles on the coating surface, and there are cracks in the molten area on the surface. The EDS element mapping of Al₂O₃ coating surface indicates that there is no other component in the coating, only Al₂O₃.
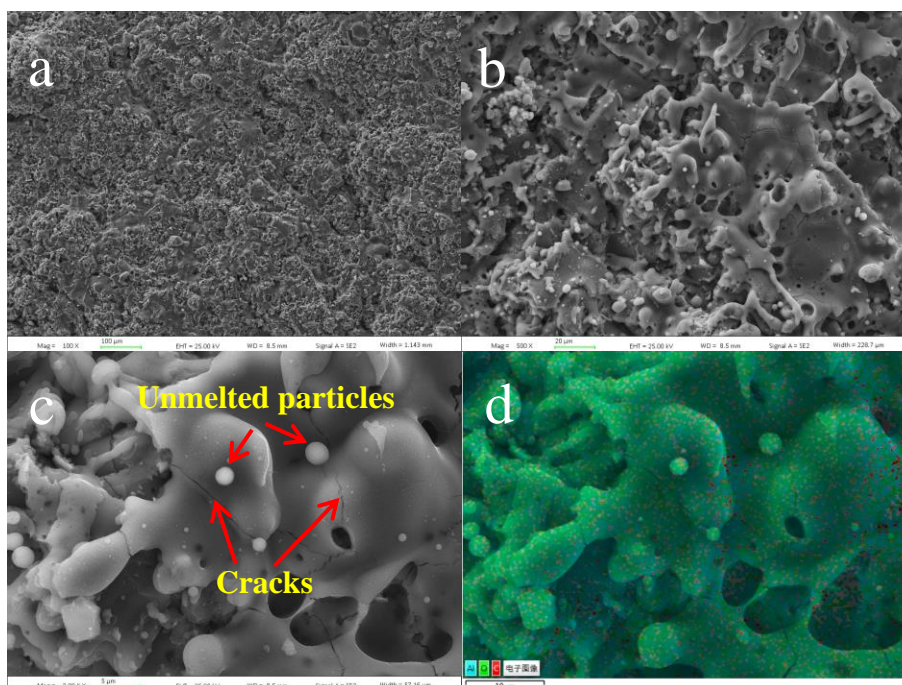

Fig. 6. SEM images of of Al₂O₃ coating surface morphology.

3.2.3. Cross section of Al₂O₃ coatings

Figure 7 shows the image of Al₂O₃ coating cross-section. The bond coat is Ni-Al. It can be seen that the bonding between Al₂O₃ coating and bond coat is good. The bonding line between the bond coat and the substrate is obvious. There are unmelted particles at the bonding interface between Al₂O₃ coating and bonding layer. Unmelted particles pile up together rather than exist as a single state. It may be due to the low external temperature of the flame flow and the incomplete melting of the powder when it strikes the substrate. Microcracks can be seen between layers. The main reason is that APS molten particles have high cooling rate and particles have obvious cooling shrinkage, which leads to overlapping and stacking layered structure in plasma-sprayed structure[23].
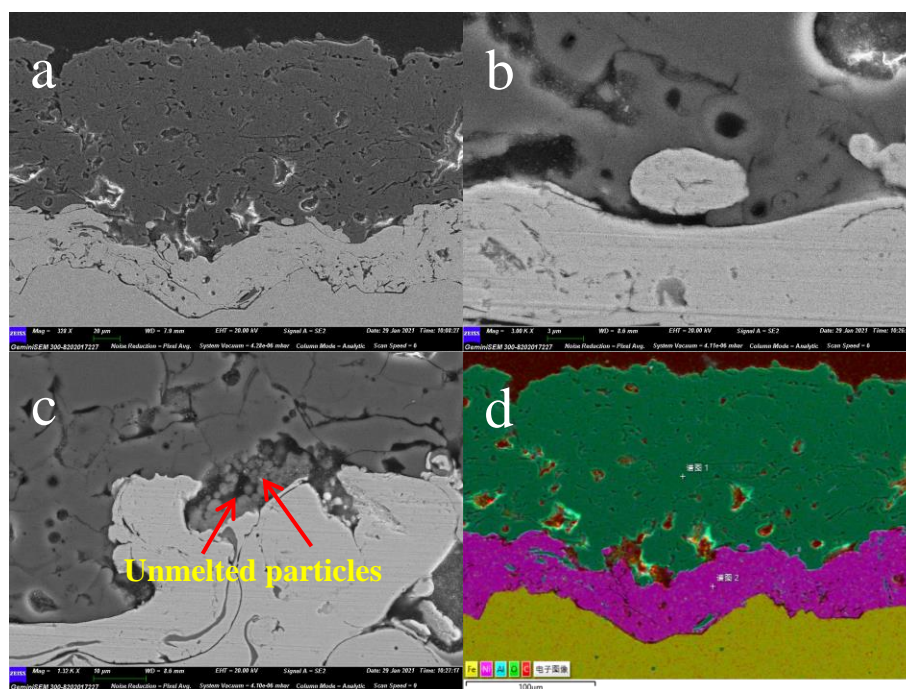
Fig. 7. Cross-section of Al₂O₃ coating.

3.2.4. XRD analysis of Al₂O₃

Figure 8 shows the XRD pattern of Al_2O_3 powder and coating prepared by APS, as well as the standard card of Al_2O_3 (PDF#89-7716) and $(Al_2O_3)_{1.333}$ (PDF#77-0396) for references. It can be seen from the figure that the main phase in the powder is Al_2O_3, which can completely match Al_2O_3 (PDF#89-7716). Al_2O_3 in the powder is mainly α-Al_2O_3. The main phase in the coating is also Al_2O_3, and part of main peaks can match $(Al_2O_3)_{1.333}$. Compared with the powder, the diffraction peaks in the coating are seriously widened, some diffraction peaks are offset, and the intensity of the derived peaks is significantly reduced. It is found that there are not only α-Al_2O_3 diffraction peak but also γ-Al_2O_3 with strong diffraction intensity in the XRD pattern of Al_2O_3 coating. This is because in the plasma spraying process, the temperature of plasma flame flow is much higher than the melting point and phase transformation temperature of Al_2O_3 powder, resulting in the phase structure of molten Al_2O_3 powder droplet changes during the deposition process of forming coating. In addition, during plasma spraying, the powder melts into liquid state at high temperature and then cools rapidly, leading to the nucleation of γ-Al_2O_3 with low nucleation free energy at the solid-liquid interface. Some partially melted and unmelted α-Al_2O_3 are retained in the coating and coexist with γ-Al_2O_3.
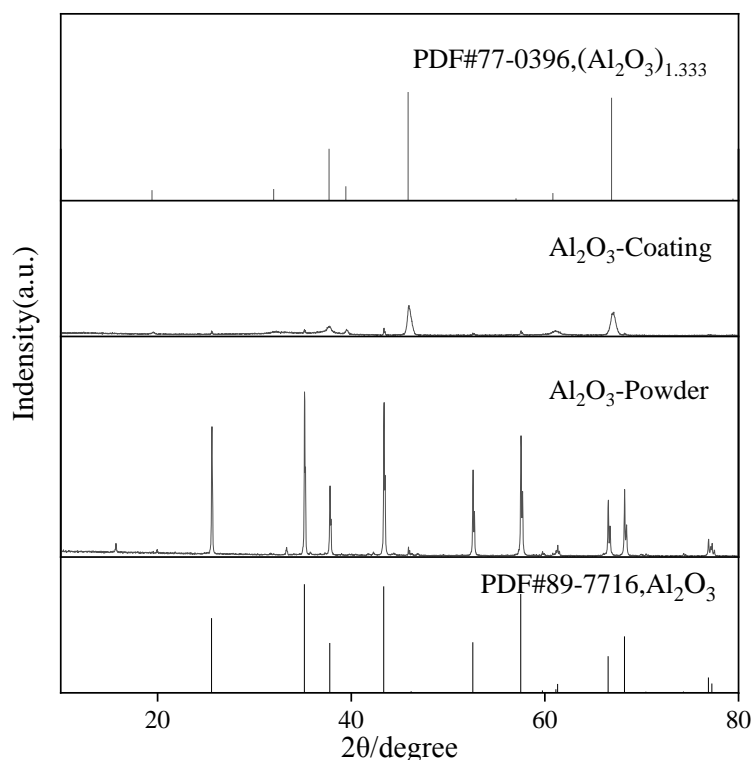
Fig. 8. XRD spectra of Al₂O₃ coating and powder.

3.3. WC-10Co4Cr

3.3.1. Morphology and composition of WC-10Co4Cr powder surface and section

Figure 9 shows the surface and cross section morphology of WC-10Co4Cr powder. It can be seen that the powder is nearly spherical or ellipsoidal and the surface is rough. WC-10Co4Cr powder was prepared by agglomerating and sintering. It is formed by agglomeration of WC particles and bonded together by CoCr bonding. The powder has good fluidity, which is convenient for the melting and deformation of the powder in the spraying process. In high temperature and high speed flame flow, spherical powders are subjected to uniform forces in the air flow, and their flight trajectories tend to be the same. The coating formed after stacking on the surface is more dense[24]. Figure 9b shows the surface morphology of WC-10Co4Cr powder under the high magnification figure. It can be seen that there are pores on the powder surface. The cross section of the powder shows that some of the powders have holes. The EDS element mapping of the powder cross section shows that WC phases are bonded by CoCr phase.
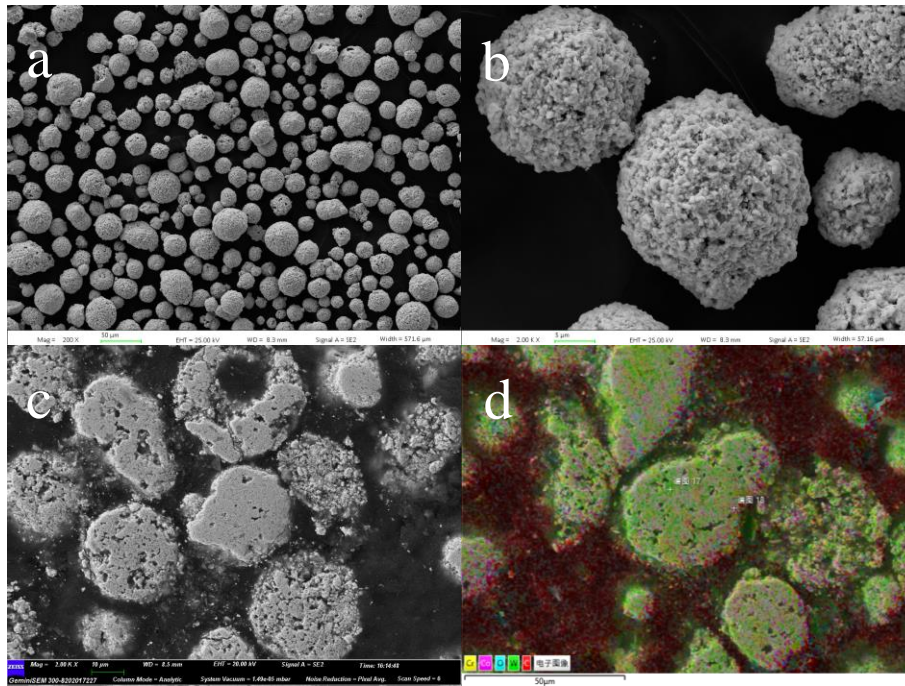
Fig. 9. SEM micrographs of WC-10Co4Cr powder.

3.3.2. Surface morphology and composition of WC-10Co4Cr coatings

Figure 10 shows the surface morphology of WC-10Co4Cr coating. At low magnification (Figure 10a), it can be seen that the coating surface is flat without fluctuation. This is because the kinetic energy of particles sprayed by HVOF is large, and the particles collide with the substrate at high speed and deform fully. Under the high magnification figure (Figure 10b-c), it can be seen that there is an obvious sense of particles on the coating surface, and some powders still remain granular. Compared with the plasma sprayed coating, the HVOF sprayed WC-10Co4Cr coating is granular. This is because the flame temperature of HVOF spraying is lower than that of plasma flame flow, but the flame flow speed is fast. When the powder particles hit the substrate surface, they are still in a semi-molten state, and only partial melting of the bonding phase CoCr occurs. Therefore, they remain granular after solidification. Figure 10d shows the EDS element mapping of WC-10Co4Cr coating. It can be seen from the figure that the components are evenly distributed, and the hard phase WC is bonded together by the bonding phase CoCr. The presence of oxygen in the coating indicates oxidation during spraying.
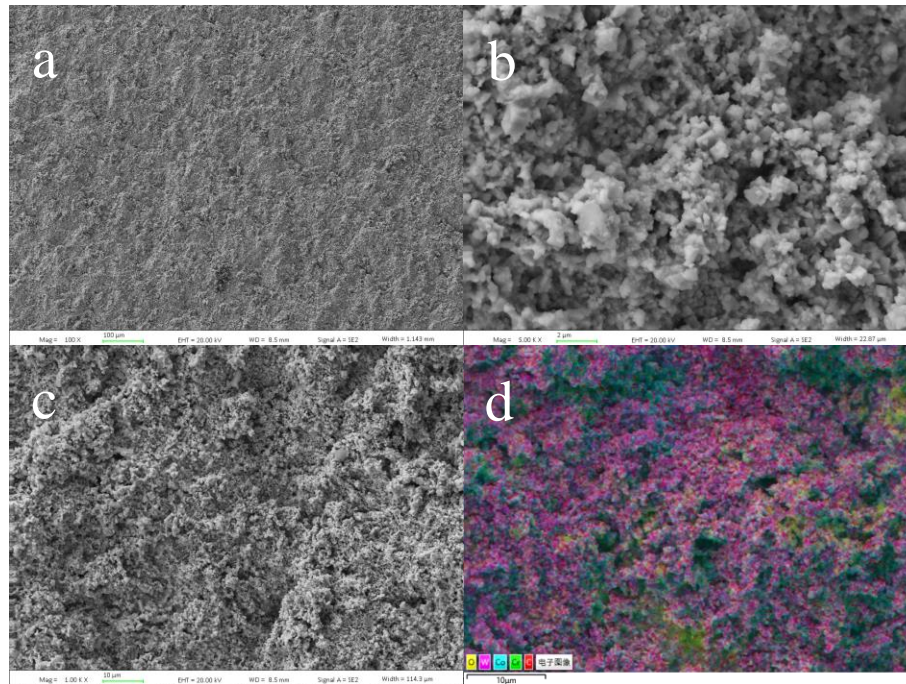
Fig. 10. SEM images of of WC-10Co4Cr coating surface morphology.

3.3.3. Cross section of WC-10Co4Cr coatings

Figure 11 shows the image of WC-10Co4Cr coating cross-section. Figure 11a shows that the bonding mode between WC-10Co4Cr coating and substrate is mechanical bite. The bonding line between the coating and the substrate is clear. Under the high magnification diagram (Figure b-c), it can be seen that the coating fits well with the substrate. This is because HVOF spraying has high particle speed and high hardness, which has a great impact on the substrate. The coating also found a small number of holes, which is due to the low flame temperature when spraying, the particle speed is fast, the powder is heated for a short time, when hitting the surface of the matrix is still in a semi-molten state, low flattening degree and formed. The EDS element mapping of WC-10Co4Cr coating shows that the coating composition is uniform. WC phase is evenly embedded in the bonding phase of Co and Cr, which ensures the high hardness and high wear resistance of the coating.
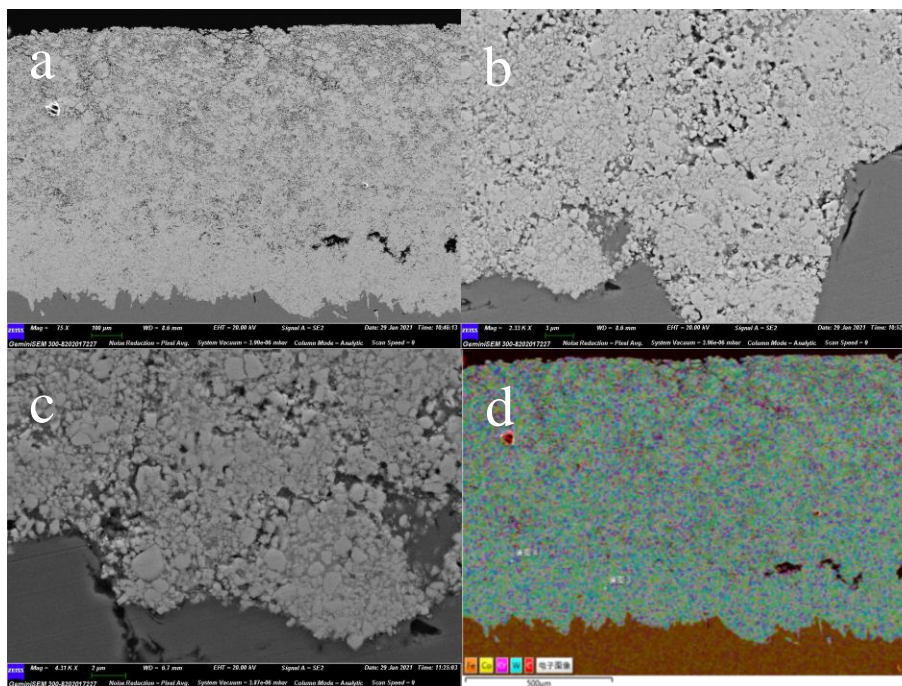
Fig. 11. Cross-section of WC-10Co4Cr coating.

3.3.4. XRD analysis of WC-10Co4Cr

Figure 12 shows the XRD pattern of WC-10Co4Cr powder and coating prepared by HVOF, as well as the standard card of WC (PDF#51-0939), W_2C (PDF#65-3896) and CrCo (PDF#09-0052) for references. The main phase in the powder is WC and a small amount of Co phase and Cr phase, which is consistent with the design composition of the powder. The phase composition of WC-10Co4Cr coating deposited by HVOF was composed of main WC and minor W_2C phase, indicating that decarbonization occurred during the spraying process. During HVOF spraying, the flame flow temperature is high, and WC-10Co4Cr powder impacts the surface of the substrate in a semi-molten state. During this process, WC contacts with oxygen in the air and oxidizes and decarbonizes, thus forming W_2C. W_2C phase has hard brittleness, and it is easier to form cracks when friction or collision occurs, resulting in coating failure. The product of decarbonization reaction has a negative effect on the coating, so it should be reduced as much as possible. This can be achieved by optimizing the spraying process, such as reducing the powder flight time and increasing the spraying speed[25]. Except for W_2C phase, the other phases in the coating are the same as the powder, which indicates that the coating prepared by HVOF spraying can exert the characteristics of the powder and obtain excellent properties of the coating. In addition, the intensity of each diffraction peak in the coating decreased, and the Co diffraction peak could not be observed. Some amorphous peaks also appeared in the coating and widened to a certain extent. This is caused by the extremely fast cooling rate after the sprayed particles are in the molten state[26]. These amorphous phases can improve the strength and hardness of the coating.
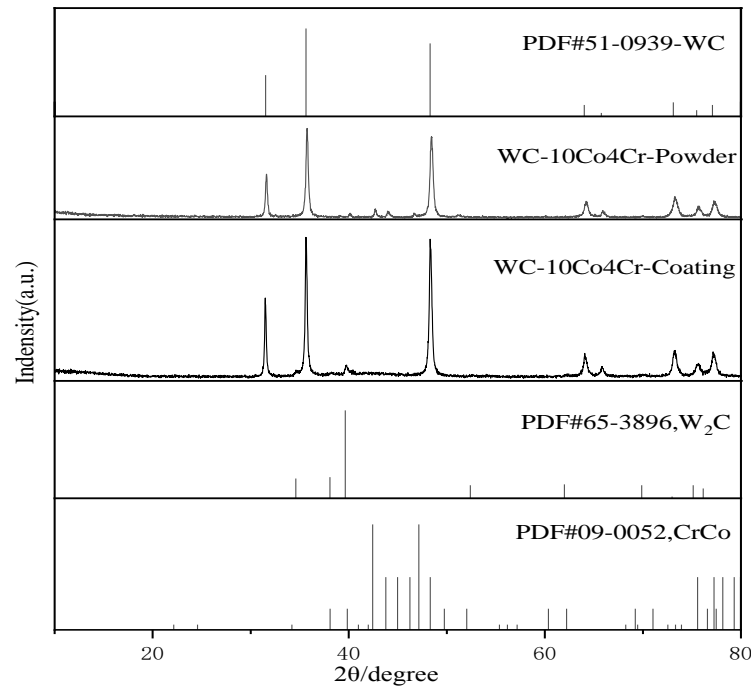
Fig. 12. XRD spectra of WC-10Co4Cr coating and powder.

3.4. Mechanical properties of coatings

Table 4 shows the Vickers hardness of the studied coatings. In terms of maximum hardness, Al_2O_3 coating has the largest hardness and WC-10Co4Cr is the smallest. In terms of average hardness, Cr_2O_3-$2TiO_2$ coating has the highest hardness and Al_2O_3 coating has the lowest hardness. Cr_2O_3-$2TiO_2$ coating and Al_2O_3 coating are ceramic coatings, so they have high microhardness. Cr_2O_3-$2TiO_2$ coating is a composite coating. Therefore, the microhardness of the coating near the hard phase Cr_2O_3 is higher and that near TiO_2 is lower. However, the alternating distribution of Cr_2O_3 and TiO_2 makes the microhardness distribution of the coating more uniform. The relative error of hardness value of Al_2O_3 coating is large, which is caused by the different melting degree of powder in the spraying process. The hardness of WC-10Co4Cr coating is relatively low due to the decarburization reaction in the spraying process.

Table 4. Vickers hardness of the studied coatings.

Coating	HV $_{max}$/HV$_{0.2}$	HV $_{avg}$/HV$_{0.2}$
Cr_2O_3	1292.3	1184.1
Al_2O_3	1354.4	1010.7
WC-10Co4Cr	1137.1	1027.3

3.5. Wear resistance of coatings

Figure 13 shows the friction coefficient curve of coatings with different pairs of grinding balls. The friction coefficient curves of different coatings obviously reflect that the whole friction and wear process can be divided into three stages: the first stage is running-in wear stage, also known as the straight-up stage; the second stage is stable wear stage; the third stage is severe wear stage[27]. The running-in wear stage is the friction stage when the grinding ball just contacts the coating surface. There are unmelted particles on the coating surface due to spraying process

problems, resulting in uneven coating surface. The presence of unmelted particles will increase the contact force with the grinding ball. In the process of reciprocating motion, the grinding ball takes the lead in grinding off the unmelted particles. The ground powder particles remain on the grinding ball or on the coating surface. The friction coefficient of the coating increases linearly with the accumulation of residual powder on the surface of the grinding ball. In the stable wear stage, the friction coefficient of the coating basically does not change dramatically. The fluctuation range of the first half of the stable wear stage is larger, which is also called the fluctuation stage, and the fluctuation range of the second half becomes smaller, which is called the stable stage. The severe wear stage is after a long period of stable wear. Due to the gap between the surfaces of the friction pair, the change of the surface morphology and the fatigue of the surface layer, the friction temperature rises rapidly and the amount of wear increases sharply.
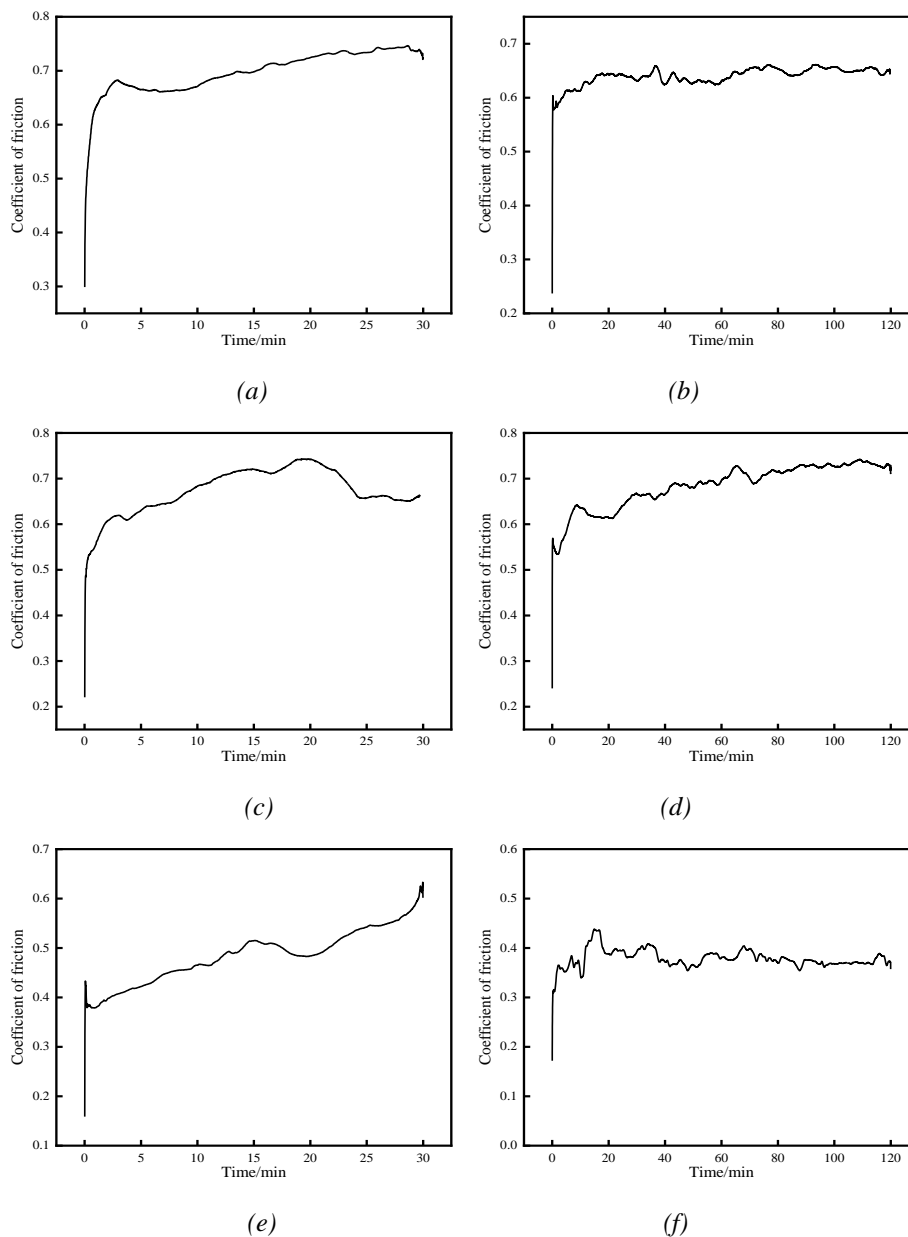

Fig. 13. Friction coefficient curves of coatings: (a) Cr_2O_3-$2TiO_2$ coating-GCr15, (b) Cr_2O_3-$2TiO_2$ coating-Si_3N_4, (c) Al_2O_3 coating-GCr15, (d) Al_2O_3 coating-Si_3N_4, (e) WC-10Co4Cr coating-GCr15, (f) WC-10Co4Cr coating-Si_3N_4.

Figure 13a shows the friction coefficient curve of Cr_2O_3-$2TiO_2$ coating with GCr15 steel for grinding ball and reciprocating friction for 30 minutes. The average friction coefficient measured by the tester is 0.699, and the friction weight loss measured by the analytical balance is 0.11 mg. It can be seen that the friction coefficient value always fluctuates throughout the reciprocating friction test, and it increases slowly as the friction time increases. Because the substrate surface is a rough and uneven original machined surface, the friction coefficient increases rapidly before 2 minutes, and serious adhesive wear occurs in this process. This process is the running-in wear stage. With the progress of friction, the adhesive wear of friction machine turns into abrasive wear, and the friction coefficient decreases accordingly. As the friction continues, the friction coefficient increases gradually. Figure 13b shows the friction coefficient curve of Cr_2O_3-$2TiO_2$ coating with Si_3N_4 for grinding ball and reciprocating friction for 120 minutes. The average friction coefficient measured by the tester is 0.640, and the friction weight loss measured by the analytical balance is 2.71 mg. Compared with the use of GCr15 steel to the grinding ball, the friction coefficient curve of the Cr_2O_3-$2TiO_2$ coating with Si_3N_4 to the grinding ball has a smaller change. After 20 minutes, it enters the stable wear stage. There is a undulating peak at about 40 minutes, which may be due to the abrasive particles falling off at the wear scar during the reciprocating friction experiment, and friction occurs as the grinding ball moves back and forth. After that, the friction coefficient no longer fluctuates greatly, and gradually tends to stable.

Figure 13c shows the friction coefficient curve of Al_2O_3 coating with GCr15 steel for grinding ball and reciprocating friction for 30 minutes. The average friction coefficient measured by the tester is 0.673, and the friction weight loss measured by the analytical balance is 0.62 mg. The friction coefficient of Al_2O_3 coating begins to decrease and enters the stable stage after going through the running-in wear stage and fluctuation stage. During the running-in wear stage of Al_2O_3 coating, the powder particles and debris on the coating surface are attached to the grinding ball surface. After entering the wear fluctuation stage, the debris will grind and fill the pores of the coating with the reciprocating friction of the grinding ball. After entering the stable stage, with the increase of friction depth, the defects of the coating are reduced accordingly, and the wear contact area between the grinding ball and the coating is reduced accordingly. Therefore, the friction coefficient of the coating is reduced. Figure 13d shows the friction coefficient curve of Al_2O_3 coating with Si_3N_4 for grinding ball and reciprocating friction for 120 minutes. The average friction coefficient measured by the tester is 0.684, and the friction weight loss measured by the analytical balance is 0.16 mg. After the running-in wear stage, the friction coefficient value fluctuates and rises. After reaching the stable stage after 80 minutes, the friction coefficient no longer fluctuates greatly, and gradually tends to be stable. Despite the reciprocating friction of 120 minutes, its wear weight loss is far less than that of Al_2O_3 coating with reciprocating friction of 30 minutes. This is due to the uneven surface hardness of the Al_2O_3 coating.

Figure 13e shows the friction coefficient curve of WC-10Co4Cr coating with GCr15 steel for grinding ball and reciprocating friction for 30 minutes. The average friction coefficient measured by the tester is 0.484, and the friction weight loss measured by the analytical balance is 0.04 mg. WC is the main component in WC-10Co4Cr coating, and WC is cemented carbide. Therefore, the phase structure formed by the coating is mainly hard phase, and CoCr exists in the form of bonding phase inside the coating. After the running-in wear stage, the friction coefficient is always rising. This is due to the large surface roughness of the coating and the presence of fine

unmelted spray powder particles, resulting in a small contact area between the coating and the grinding ball, so the friction coefficient increases. It also shows that 30 minutes of reciprocating friction is not enough to make the coating enter a stable wear stage. Figure 13f shows the friction coefficient curve of WC-10Co4Cr coating with Si_3N_4 for grinding ball and reciprocating friction for 120 minutes. The average friction coefficient measured by the tester is 0.379, and the friction weight loss measured by the analytical balance is 0.21 mg. After the straight-up stage, the friction coefficient of the WC-10Co4Cr coating decreases. This is due to the existence of pores in the WC-10Co4Cr coating, which cannot be avoided during the spraying process. Then the friction coefficient increases. This is because the CoCr bonding phase on the surface of WC-10Co4Cr coating is worn first. Exposed WC hard particles will hinder relative sliding, resulting in the increase of friction coefficient. After entering the fluctuation stage, the friction coefficient curve fluctuates within a certain range, which is caused by the uneven distribution of the WC hard phase inside the coating. The bonding phase CoCr is squeezed into the WC hard phase due to external pressure. After 60 minutes, the bonding phase was gradually squeezed to a saturated state. The area of the grinding ball in contact with the bonding phase is reduced, and the area in contact with the hard phase is increased. Therefore, the friction coefficient curve of the coating has smaller fluctuations and tends to be flat. With the progress of reciprocating friction, the thermal effect of friction is more significant, and oxidation products with a certain anti-friction effect are generated[28], so the friction coefficient is reduced.

The friction coefficient curve and wear amount of the three wear-resistant coatings are analyzed and compared. When the friction pair adopts GCr15 steel and reciprocating friction for 30 minutes, the average friction coefficient and wear amount of Al_2O_3 coating are the largest. The average friction coefficient and wear amount of WC-10Co4Cr coating are the smallest. In this regard, the wear resistance of WC-10Co4Cr coating is the best. When Si_3N_4 is adopted for the friction pair and the reciprocating friction is 120 minutes, the average friction coefficient of Al_2O_3 coating is the largest, but the wear amount is the smallest. The wear amount of Cr_2O_3-2TiO_2 coating is the largest and far exceeds that of the other two coatings. Considering the average friction coefficient and wear amount of the three coatings comprehensively, the wear resistance of the WC-10Co4Cr coating is the best. This is because WC-10Co4Cr coating adds Cr on the basis of WC-Co, and the CoCr bonding phase formed by the coating can inhibit WC decarburization and reduce the formation of W. Therefore, WC-10Co4Cr coating has less friction loss and better wear resistance.

4. Conclusions

The wear-resistant coatings of Cr_2O_3-2TiO_2, Al_2O_3 prepared by APS and WC-10Co4Cr prepared by HVOF were studied and compared.

Cr_2O_3-2TiO_2 coating is a typical plasma-sprayed coating. The spray particles spread well and the flattening degree is high. Because the crystal structure of Cr_2O_3 is the same as that of α-Al_2O_3, the structure of Cr_2O_3-2TiO_2 coating prepared by APS is stable without phase transformation.

Al_2O_3 coating has the stacking structure of plasma-sprayeed coating. The surface of coating is relatively flat and the density is high. It can be seen that the bonding between Al_2O_3

coating and bond coat is good, but microcracks can be seen between layers. Compared with the powder, the diffraction peaks in the coating are seriously widened, some diffraction peaks are offset, and the intensity of the derived peaks is significantly reduced. The phase structure of molten Al_2O_3 powder droplet changes during the deposition process of forming coating. Therefore, there are not only α-Al_2O_3 diffraction peak but also γ-Al_2O_3 with strong diffraction intensity in the XRD pattern of Al_2O_3 coating

The surface of WC-10Co4Cr coating has obvious graininess, and some powders still remain granular. The presence of oxygen in the coating indicates oxidation during spraying. WC phase is evenly embedded in the bonding phase of Co and Cr, which ensures the high hardness and high wear resistance of the coating. The phase composition of WC-10Co4Cr coating deposited by HVOF was composed of a main WC and minor W_2C phase, indicating that decarbonization occurred during the spraying process. In addition, the intensity of each diffraction peak in the coating decreased, and the Co diffraction peak could not be observed.

The average hardness of Cr_2O_3-$2TiO_2$ coating is the highest and that of Al_2O_3 coating is the lowest. The relative error of hardness value of Al_2O_3 coating is large due to the different melting degree of powder in the spraying process. Due to the decarburization reaction in the spraying process, the hardness of WC-10Co4Cr coating is relatively low. WC-10Co4Cr coating adds Cr on the basis of WC-Co, and the CoCr bonding phase formed by the coating can inhibit WC decarburization and reduce the formation of W. Therefore, after comprehensively comparing the average friction coefficient and wear amount of the three coatings, the wear resistance of the WC-10Co4Cr coating is better.

Acknowledgements

References

[1] L. Chen , G. J. Yang , Ch. X. Li et al., Advanced Ceramics **1**, 3 (2016)
[2] J. J. Bai, Dalian University of Technology, (2012)
[3] Y. Ren , X. Ch. Lu , Y. Huang, Heat Treatment **1**, 12 (2009)
[4] G. M. Xia , J. Q. Zhou , X. B. Min, Metal Materials and Metallurgy Engineering **1**, 53 (2012)
[5] Y. Cui , F. Lin , X. J. Song et al., Nonferrous Metals **S1**, 65 (2006)
[6] B. S. Xu , S. H. Zhu , Theories and Technologies on Surface Engineering, (1999)
[7] C. X. Hu, Fundamentals and Application of Thermal Spraying, (1994)
[8] J. K. Murthy , D. S. Rao , B. Venkataraman, Wear 249(7), 592 (2001); https://doi.org/10.1016/S0043-1648(01)00682-2
[9] P. Fauchais , Journal of Physics D Applied Physics 37(37), 86.(2004); https://doi.org/10.1088/0022-3727/37/9/R02
[10] J. Zhang , Y. H. Niu, Ordnance Material Science and Engineering **41**(04), 76 (2018)
[11] G. Li , T. Dong , H. Wang et al., Materials and Design 88(5), 906 (2015);

https://doi.org/10.1016/j.matdes.2015.09.085

[12] D. P. Weston , P. H. Shipway , S. J. Harris, Wear 267(5), 934 (2009);
https://doi.org/10.1016/j.wear.2009.01.006

[13] R. J. K. Wood , S. Herd , M. R. Thakare, Tribology International 119, 491 (2018);
https://doi.org/10.1016/j.triboint.2017.10.006

[14] G. Xie, X. Song, D. Zhang et al. Applied Surface Science 256(21), 6354 (2010);
https://doi.org/10.1016/j.apsusc.2010.04.016

[15] J. M. Marshall , M. Giraudel, International Journal of Refractory Metals and Hard Materials
49, 57 (2015); https://doi.org/10.1016/j.ijrmhm.2014.09.028

[16] T. Sudarpasert , P. H. Shipway , D. G. Mccartney, Wear 255(7), 943 (2003);
https://doi.org/10.1016/S0043-1648(03)00293-X

[17] V. A. D. Souza, A. Neville, Journal of Thermal Spray Technology 15(1), 106 (2006);
https://doi.org/10.1361/105996306X92677

[18] J. E. Cho, S. Y. Hwang, K.Y. Kim, Surface and Coating Technology 200(8), 2653 (2006);
https://doi.org/10.1016/j.surfcoat.2004.10.142

[19] Ch. J. Chen et al., Surface Technology **48**(09), 224 (2019)

[20] H. M. Liu, Equipment Environmental Engineering **14**(09), 6 (2017)

[21] D. I. Pantelis , P. Psyllaki, N. Alexopoulos, Wear 237(2), 197 (2000);
https://doi.org/10.1016/S0043-1648(99)00324-5

[22] R. Z. Li et al., SURFACE TECHNOLOGY 50(09), **184** (2021)

[23] Z. P. Zhao, H. L. Si, Zh. Sh. Li et al., Surface Technology **48**(08), 225 (2019)

[24] Y. P. Song, Nanjing University Of Aeronautics And Astronautics, (2018)

[25] J. Zhao, X. M. Chen, L. Fu et al., Corrosion & Protection **41**(05), 1 (2020)

[26] Q. Wang, Sh. Y. Zhang et al., Surface and Coatings Technology 218, 127 (2013);
https://doi.org/10.1016/j.surfcoat.2012.12.041

[27] J. F. Ni et al., Surface Technology **47**(03), 210 (2018)

[28] P. B. Mi, T. Wang, F. X. Ye, International Journal of Refractory Metals and Hard Materials
69, 158 (2017); https://doi.org/10.1016/j.ijrmhm.2017.08.012